Responses to Transients in Living and Simulated Neurons

Michael Stiber, *Member, IEEE*, Ricci Ieong, and José P. Segundo

Brief Paper

Abstract

This paper is concerned with synaptic coding when inputs to a neuron change over time. Experiments were performed on a living and simulated embodiment of a prototypical inhibitory synapse. These were used to test a simple model composed of a fixed delay preceding a nonlinear encoder. Based on these results, we present a qualitative model for phenomena previously observed in the living preparation, including hysteresis and dependence of discharge regularity on rate of change of presynaptic spike rate. As change is the rule rather than the exception in nature, understanding neurons' responses to nonstationarity is essential for understanding their function.

Keywords

Synaptic coding, transients, dynamics.

I. Introduction

Changes are ubiquitous in nature; survival depends on our ability to cope with them. These changes must necessarily be reflected in changing spike trains of the neurons which encode them, if they are to have any effect on behavior. One simple type of changing discharge is that associated with unidirectional muscle movement, which may produce accelerating or decelerating *transients*. Despite the importance of neuron transient responses, until recently they have been understood only superficially [1].

This communication continues previous work which involved a prototypical living inhibitory synapse: the crayfish slowly adapting stretch receptor organ (SAO). This has been concerned with presynaptic discharges with interspike interval timings that have patterns with trends [2] — either accelerating or decelerating monotonically. These transients are among the simplest nonpacemaker input regimes allowing examination

Support for this work was provided by the Hong Kong Research Grants Council (CERG HKUST187/93E).

M. Stiber is with the Department of Molecular & Cell Biology, 315 Life Sciences Addition, University of California, Berkeley, CA 94720-3200 USA. E-mail: stiber@cicada.berkeley.edu.

R. Ieong is with the Department of Computer Science, The Hong Kong University of Science & Technology, Clear Water Bay, Kowloon, Hong Kong. E-mail: ricci@cs.ust.hk.

J.P. Segundo is with the Department of Neurobiology, and Brain Research Institute, University of California, Los Angeles, CA, 90025-1763 USA. E-mail:segundo@neurobio.medsch.ucla.edu

of nonstationary synaptic coding, and are also reasonable models for neural input in sensorimotor systems during motor activity. We wish to understand how neural responses to changing input compare to that to stationary input, and propose a general model for this.

Here we expand on experiments on the living preparation with simulations of a physiological neural model. The preparation includes the recognized prototype of an inhibitory synapse, and results obtained from it should be considered valid for any such synapse as a working hypothesis at least [3]. Results from the living preparation led to the hypothesis that much of the cell's behavior could be explained as the action of a "first order lead-lag" system; our simulations allow us to test this.

II. A Prototypical Inhibitory Synapse

Figure 1 about here.

The experimental setup for the SAO is diagrammed in Fig. 1 (left) [4]. It includes a presynaptic inhibitory fiber (IF) and a postsynaptic neuron. In the absence of stimulation, the IF is quiescent and the postsynaptic cell fires as a *pacemaker*, with all interspike intervals practically equal to N, its *natural* interval [4]. Stimulation and recording was accomplished by a pair of electrodes — the former eliciting action potentials (APs) in the IF which traveled to its synapse with the postsynaptic cell, and the latter capturing both presynaptic and postsynaptic events which were separated by their differing amplitudes [4].

The model shown in Fig. 1 (right) was originally developed by Edman and collaborators to model interspike timing in the lobster stretch receptor organs [5]; we assume that inter-species differences are minimal. Two modifications of the original model were incorporated (equations are presented in appendix A):

1. A *pacemaker potential* was added as a bias current I_{bias} (1) to produce pacemaker firing as in the SAO.
2. A simple *inhibitory synapse* model was incorporated as I_{syn} (1, 6). This causes a brief change in cell membrane permeability to Cl^- ions in response to an arriving spike [6].

Model parameters were adjusted as follows: First, a range was determined for I_{bias} that produced pacemaking behavior with a physiologically realistic range [4]. Second, the synapse parameters were set such that modeled postsynaptic potentials fit those noted in the literature for the SAO [3], [6]. At no time were parameters modified in an attempt to match synaptic coding in the model to that observed in the SAO — any similarity stems from the structural correspondence between the two systems.

A. Transient Generation and Data Analysis

Figure 2 about here.

A detailed description of the experimental procedures with respect to the experiments on the SAO is available elsewhere [2]; we summarize the relevant aspects here and in Fig. 2. Transients were those in which the instantaneous input rate (reciprocal of interspike interval) changed monotonically according to an experimenter-selected waveform (a ramp in this case). A single experiment involved a series of accelerating and decelerating transients separated by gaps, G, long enough for each transient to be isolated from the aftereffects of the previous one. Fig. 2(A) shows the *rate control waveform*, $r(t)$, which determined the desired instantaneous input rate as a function of time. Each transient had a duration or *span*, S, and start and end rates r_{start} and r_{end}.

The times of occurrence of certain events were pertinent. The beginning of each symmetrical pair of transients was indicated by a *cycle marker*, as in Fig. 2(B), at time c_j ($j = 1, 2, \ldots$). Presynaptic spikes occurred at times s_k (Fig. 2(C)), computed in the simulation by $s_k = s_{k-1} + 1/r(s_{k-1})$ ($k = 1, 2, \ldots$). Times of postsynaptic spikes were recorded at times t_i ($i = 1, 2, \ldots$, Fig. 2(D)).

Analysis was based on interspike intervals and cross intervals. As shown in Fig. 2(C,D), these were: *presynaptic intervals* $I_k = s_k - s_{k-1}$, *postsynaptic intervals* $T_i = t_i - t_{i-1}$, *phases* $\phi_i = t_i - s_*$ (cross interval from postsynaptic event i back to the most recent preceding presynaptic event), and also *cross intervals* $\psi_k = s_k - c_*$ and $\psi_i = t_i - c_*$ (from a pre- or postsynaptic event, respectively, back to the most recent preceding cycle marker).

B. Responses to Pacemaker Inputs

The stationary responses of a neuron to pacemaker input ($\forall k, I_k = I$) have been analyzed using point process mathematics [7] and nonlinear dynamics [8] techniques [4], [9]; we briefly summarize background necessary for this treatment.

A spike train's temporal pattern — represented equivalently by the sequence of spike times or intervals (e.g., $\langle \ldots, T_i, T_{i+1}, \ldots \rangle$) — reflects the evolution of the internal state of the neuron along time: spikes are only produced when the state traverses some limited part of its state space, and their timing indicates the time the system takes to return to that region. Discharge patterns can be used to identify system activity as belonging to universal behavioral categories experimentally identified in nonlinear dynamical systems in diverse fields [8], [10]. From most regular to least, these behaviors include: locked or alternating, intermittent, and "messy" (either chaotic or stochastic). Distinguishing between alternating and non-alternating behaviors is sufficient for our purposes here.

If all T_i are equal to their mean, $\bar{T}$, one can infer that the system state is *periodic* (in this case period 1), tracing out some closed *limit cycle* in its state space. More generally, in the case of pacemaker driving and taking into account the temporal relationship between the presynaptic and postsynaptic trains, a periodic behavior is one in which a sequence of intervals $\langle T_i, T_{i+1}, \ldots, T_{i+q-1} \rangle$ and phases $\langle \phi_i, \phi_{i+1}, \ldots, \phi_{i+q-1} \rangle$ repeat unceasingly ($T_i = T_{i+q}$, $\phi_i = \phi_{i+q}$) in the same time it takes p presynaptic spikes to occur ($pI = q\bar{T}$). We call this *p:q locking*, where there are p presynaptic spikes for the q postsynaptic ones in a sequence (p, q integers). Fig. 2(E) schematizes a 2:1 locking (2 presynaptic spikes for each postsynaptic one).

Locking can be generalized to include the case of nonstationary stimuli; this is *p:q alternation*. Here, there is still a fixed relationship between p pre- and q postsynaptic events, but a trend is imposed upon the sequence of postsynaptic intervals by the trend of the presynaptic transient. Locking is the stationary form of alternation. Fig. 2(F) illustrates 1:1 alternation with a decelerating presynaptic discharge.

A variety of non-alternating behaviors are produced in response to stationary or monotonic transient driving. It will become clear in the following section that they are easily distinguished from alternation.

III. Responses To Transients

Figure 3 about here.

The *pooled graphs* in Fig. 3 compare SAO and model responses to a slowly accelerating ramp transient. They show only those intervals or phases whose reference events (at t_i) occurred within the transients' spans, in other words, they are plots of the points (ψ_i, ϕ_i) for $0 \leq \psi_i \leq S/2 - G$. A pooled graph can be considered a *bifurcation diagram* [10]: a plot of neuron behavior versus a control parameter [11]. In a pooled graph, this control parameter is the time since the beginning of a transient, ψ_i, which maps (linearly, in the case of a ramp transient) to instantaneous presynaptic rate.

In both of the graphs, the plotted points form patterns along the ordinate which change abruptly at certain abscissa values. These values of ψ_i are *bifurcation points*, where qualitatively distinct behaviors some together. For example, in Fig. 3 bifurcation points bounding 1:1 alternation are marked by vertical lines; the alternation itself is revealed by the single category of phases which exists between these two values of ψ_i. Beyond the bifurcation points in either direction lie behaviors other than 1:1 alternation, including non-alternating behaviors and *p:q* alternations ($p < q$ to the left of 1:1, $p > q$ to the right for an accelerating transient).

Generally speaking, the simulation reproduces the major features observed in the SAO, including:

- The monotonically changing input is coded into a nonmonotonic output.
- When the output does change monotonically (for instance, during 1:1 alternation), it is in the same sense as the input (both accelerating or both decelerating).
- There is a clear correspondence between the bifurcations under transient driving and those resulting from pacemaker driving, as will be shown shortly.
- The exact location of bifurcation points between behaviors, and the existence of some of the behaviors, depends on the sign and magnitude of the transient *slope*, $m = \mathrm{d}r(t)/\mathrm{d}t$ (constant for ramp transients).

Figure 4 about here.

This final point is the source of a *hysteresis effect*, illustrated by Fig. 4, which shows responses to symmetrical, moderately fast ($m = 4/\mathrm{s}^2$) transients. The decelerating transient response (bottom) is plotted with a reversed X axis, so corresponding locations on the X axes of each graph indicate equal instantaneous presynaptic rates. It is readily apparent to the naked eye that the bifurcations bounding 1:1 alternation occur at lower rates for a decelerating transient than for an accelerating one; the same is true for the other bifurcations.

In the SAO, this had previously been attributed to the neuron behaving approximately as a "first order lead-lag" system [2]. This is equivalent to hypothesizing that the cell can be modeled by a fixed delay δ, the output of which is passed to a nonlinear dynamical system which "selects" a behavior in response to the instantaneous rate of the delayed input. Such a system would exhibit hysteresis, and δ could be determined by fitting a line to the plot of any bifurcation point set versus m. If the linear fit is not acceptable for any bifurcation, or the δ computed is not constant over all, then this hypothesis must be rejected.

Figure 5 about here.

Pooled graphs were plotted and, using custom MATLAB software, bifurcation points were identified by hand and indicated ψ_i values were converted to rates. Fig. 5 shows the bifurcation points bounding 1:2, 1:1, and 2:1 alternations (near 5–6/s, 8–12/s, and 16–19/s, respectively) for accelerating and decelerating ramp transients plotted versus $|m|$. Lines of best fit are also plotted. As slopes increase, points' locations on the rate scale increase for accelerating transients and decrease for decelerating ones. The difference between bifurcation point location for positive versus negative slope results in hysteresis, indicated by H in the figure for $|m| = 2/\mathrm{s}^2$.

Table 1 about here.

Computed values of δ, along with y-intercepts, actual bifurcation points, and correlation coefficients, are presented in Table I.

IV. Discussion

It is important to reiterate the fact that the well-known nonlinear nature of synaptic coding is manifested here in the nonmonotonic responses of both the SAO and the model to smooth, monotonically changing input transients. This is a consequence of the bifurcation behavior of general nonlinear dynamical systems. Furthermore, recognition of these bifurcation points and identification of the behaviors they bound does not require statistical tests: they are universal dynamical behaviors defined in terms of the topology of the manifold on which the system's state evolves and are reflected in the pattern of interspike intervals and phases produced by the neuron and model. It is also significant to note also that the parameters of the simulation were *not* adjusted to duplicate the behaviors produced by the SAO; they were set to match its detailed physiological characteristics.

For slowly-changing, gradual transients ($|m|$ small), the responses approximate the global behavior observed under stationary driving within the same range of input rates. As $|m|$ increases, however, the neuron's responses increasingly depart from the stationary bifurcation behaviors, showing dependence on the magnitude of the rate of change of instantaneous input rate and asymmetric sensitivity to its sign (hysteresis). Behaviors still correspond to stationary ones (low-ratio alternations being the most easily compared), but some of the stationary ones are lost (such as 1:2 and 2:1 alternation for $|m|$ much larger than $4/\mathrm{s}^2$).

As indicated in Table I, the relationship between bifurcation point and slope m is quite linear. However, the delays δ computed for each bifurcation are *not* equal: each bifurcation appears to have its own characteristic δ. Generally, the low-rate alternation boundaries are associated with larger delays for accelerating inputs and smaller delays for decelerating ones.

The computed y-intercepts are estimates of the stationary (m=0) bifurcation point locations; that they bracket the actual values suggests a nonlinear dependence on slope for very small m. We must therefore reject any simple, contant-delay-based model for the response of this cell to input transients. **Figure 6 about here.**

Lacking an analytic model for transient responses, we may still make use of a qualitative one. We visualize the relationship between stationary and transient behaviors using a Z^n (or *staircase*) formulation: a generalization of the "ZZ-switch" hysteresis curve [12], represented schematically in Fig. 6. In this figure, each "tread" of the staircase corresponds to a family of qualitatively similar neural behaviors, the "risers" are the bifurcations from one behavior type to the next, and the horizontal axis is input rate. As the input rate changes monotonically, the system will shift from one tread to the next as the rate moves past each tread's edge.

For stationary driving, the risers form right angles to the treads. As $|m|$ increases, the "tops" of the risers move to the right, and the "bottoms" move to the left, resulting in each tread overlapping the one below it (as shown in the figure). The amount of shift is described by the curves in Fig. 5. Thus, hysteresis is the result of the difference between riser tops and bottoms: with acceleration, the system's shifts are determined by the tops; with deceleration, by the bottoms. Furthermore, the amount of tread overlap can explain how behaviors are abolished via two mechanisms: **1.** if one tread completely overlaps the next, then the system will "skip it", **2.** even if complete overlap doesn't occur, the residence time of the system on a tread may be insufficient for its state to approach the dynamical attractor which defines that behavior.

V. Conclusion

Responses of a living and model neuron to monotonically changing ramp transients have been presented, along with a qualitative explanatory model for their sensitivity to the sign and magnitude of transient slope. This analysis was based on the information contained in the interspike intervals of the postsynaptic neuron, which is precisely the information transmitted across any chemical synapse. In principle then, a neuron should be able to respond to its input as though it were "diagnosing" the dynamical laws being obeyed by others presynaptic to it. These behaviors would serve as the basis of communication among neurons [2].

Though still preliminary, it is important to note that this formulation does not depend on the exact quantitative relationship in Fig. 5; *any* nonlinear system which has an internal state that lags changing inputs by at least a constant delay should be expected to exhibit similar responses. This is the subject of experimental, simulation, and formal work currently in progress which will extend understanding to other monotonic transients.

Acknowledgments

The authors would like to thank Bilin Stiber, Dominic Lai, and Ng Ka Ho for their help in this project.

References

[1] B. Huberman and W. Wolff, "Finite precision and transient behavior," *Phys. Rev. A*, vol. 32, pp. 3768–70, 1985.

[2] J. Segundo, M. Stiber, E. Altshuler, and J.-F. Vibert, "Transients in the inhibitory driving of neurons and their post-synaptic consequences," *Neurosci.*, vol. 62, no. 2, pp. 459–80, 1994.

[3] S. W. Kuffler and C. Eyzaguirre, "Syanptic inhibition in an isolated nerve cell," *J. Gen. Physiol.*, vol. 39, no. 1, pp. 155–84, 1955.

[4] J. P. Segundo, E. Altshuler, M. Stiber, and A. Garfinkel, "Periodic inhibition of living pacemaker neurons: I. Locked, intermittent, messy, and hopping behaviors," *Int. J. Bifurcation and Chaos*, vol. 1, pp. 549–81, Sept. 1991.

[5] A. Edman, S. Gestrelius, and W. Grampp, "Analysis of gated membrane currents and mechanisms of firing control in the rapidly adapting lobster stretch receptor neurone," *J. Physiol.*, vol. 384, pp. 649–69, 1987.

[6] K. Ozawa and K. Tsuda, "Membrane permeability change during inhibitory transmitter action in crayfish receptor cell," *J. Neurophysiol.*, vol. 36, no. 5, pp. 805–16, 1973.

[7] D. Cox and V. Isham, *Point Processes.* London: Chapman and Hall, 1980.

[8] R. Abraham and C. Shaw, *Dynamics — The Geometry of Behavior*, vol. 1–4. Santa Cruz, Calif.: Aerial Press, 1984.

[9] M. Stiber, K. Pakdaman, J.-F. Vibert, E. Boussard, J. Segundo, T. Nomura, S. Sato, and S. Doi, "Complex responses of living pacemaker neurons to pacemaker inhibition: a comparison of dynamical models," *Biosystems*, vol. 40, pp. 177–88, 1996.

[10] P. Bergé, Y. Pomeau, and C. Vidal, *Order Within Chaos: A Deterministic Approach to Turbulence.* New York: Wiley, 1986.

[11] J. Segundo, J.-F. Vibert, and M. Stiber, "Periodically modulated inhibition and its post-synaptic consequences. III. The heterogeneity of the postsynaptic spike trains and how several control parameters affect it," *Neurosci.*, submitted, 1997.

[12] B. Deng, "Constructing homoclinic orbits and chaotic attractors," *Int. J. Bifurcation and Chaos*, vol. 4, no. 4, pp. 823–41, 1994.

[13] A. Hodgkin and A. Huxley, "A quantitative description of membrane current and its application to conduction and excitation in nerve," *J. Physiol. (Lond.)*, vol. 117, pp. 500–44, 1952.

Appendix

I. Permeability Model Equations

The physiological model chosen was initially developed by Edman, Gestrelius, Grampp, and Sjölin for the lobster SAO and FAO (fast adapting stretch receptor organ) [5]. Ionic fluxes are explicitly represented, and regulated by membrane permeabilities. Two of these fluxes, Na^+ and K^+, are controlled by voltage-sensitive permeabilities, P_{Na} and P_K (2, 3). Three leakage permeabilities, $P_{L,Na}$, $P_{L,K}$, and $P_{L,Cl}$, present constant pathways for Na^+, K^+, and Cl^- fluxes, respectively (4). Two active pumping pathways, $I_{p,Na}$ and $I_{p,K}$ work to maintain internal ionic concentrations (5). As in the Hodgkin-Huxley (H-H) model [13], the membrane also has an associated capacitance, C_m (1).

Two additions were made to the basic model — a bias current which reproduces the pacemaking behavior of the living cell (1), and a synaptic channel (6). Inputs from the presynaptic cell cause fixed-duration changes in the synaptic permeability, P_{syn}, to Cl^- [6]. Ionic fluxes are dependent not only on the membrane potential, but also on the transmembrane concentration differential. The membrane potential equation is presented in equation (1), where the currents I_{X} (for type X) are computed from ionic fluxes as shown in (2–6).

$$
\begin{aligned}
\mathrm{d}V_m/\mathrm{d}t &= -(I_{\text{Na}} + I_{\text{K}} + I_{\text{L,Na}} + I_{\text{L,K}} + I_{\text{L,Cl}} + I_{\text{p}} + I_{\text{bias}} + I_{\text{syn}})/C_m && (1)\\
I_{\text{Na}} &= A\bar{P}_{\text{Na}} m^2 hl \frac{V_m F^2}{RT} \frac{[\text{Na}^+]_o - [\text{Na}^+]_i \exp FV_m/RT}{1 - \exp FV_m/RT} && (2)\\
I_{\text{K}} &= A\bar{P}_{\text{K}} n^2 r \frac{V_m F^2}{RT} \frac{[\text{K}^+]_o - [\text{K}^+]_i \exp FV_m/RT}{1 - \exp FV_m/RT} && (3)\\
I_{\text{L,X}} &= AP_{\text{L,X}} \frac{V_m F^2}{RT} \frac{[X]_o - [X]_i \exp(FV_m/RT)}{1 - \exp(FV_m/RT)} && (4)\\
I_{\text{p}} &= \frac{AF}{3} \frac{\bar{J}_{\text{p,Na}}}{\left(1 + \frac{K_m}{[\text{Na}^+]_i}\right)^3} && (5)\\
I_{\text{syn}} &= A\bar{P}_{\text{syn}} \frac{V_m F^2}{RT} \frac{[\text{Cl}^-]_o - [\text{Cl}^-]_i \exp FV_m/RT}{1 - \exp FV_m/RT} \times \sum_{\forall s_k < t} (e^{(s_k - t)/\tau_+} - e^{(s_k - t)/\tau_-}) && (6)
\end{aligned}
$$

Here A is the cell membrane area, the $\bar{P}_{\text{X}}$ are the maximum permeabilities, F is the Faraday constant, R is the universal gas constant, T is absolute temperature, and m, h, l, n, and r are gating variables similar in concept to those of the H-H model. The variables m, h, and l are the fast activation, fast inactivation, and slow inactivation, respectively, for P_{Na}. For P_{K}, n is fast activation, and r is slow inactivation. The pumping mechanism exchanges 3 Na^+ ions for 2 K^+ in (5), where $\bar{J}_{\text{p,Na}}$ is the maximum Na^+ pump capacity, K_m is a constant, and the factor of 1/3 is the net effect of the 3:2 pump ratio.

The synaptic current (6) is produced by a transient change in the membrane permeability to Cl^- ions. The time course of this change is fixed in relation to the arrival time s_k of each input spike. The partial change produced by each arrival is summed to produce the overall effect.

For our purposes, $[\text{Cl}^-]_i$, $[\text{K}^+]_i$, and $[\text{Na}^+]_i$ are assumed constant. The gating variables' kinetics are defined by a first-order equation (7) (where $g \in \{m, h, l, n, r\}$), with the asymptotic values g_∞ and the time constants τ_g given by (8) and (9).

$$
\begin{aligned}
\mathrm{d}g/\mathrm{d}t &= (g_\infty - g)\frac{1}{\tau_g} && (7)\\
g_\infty &= \nu_g + \frac{1-\nu_g}{1+\exp\left[\frac{z_g e}{kT}(V_m - V_g)\right]} && (8)\\
\tau_g &= \frac{Q_g \bar{\tau}_g}{\exp\left[\frac{\delta_g z_g e}{kT}(V_m - V_g)\right] + \exp\left[\frac{(\delta_g - 1) z_g e}{kT}(V_m - V_g)\right]} && (9)\\
Q_g &= \left(\frac{1-\delta_g}{\delta_g}\right)^{\delta_g} + \left(\frac{1-\delta_g}{\delta_g}\right)^{\delta_g - 1}
\end{aligned}
$$

In these expressions, ν_g is the minimum value of the relative channel permeability, z_g the effective valency of the gating structure, e the electron charge, V_g the membrane voltage at which half of the gating system is in its "open" state, $\bar{\tau}_g$ the maximum value of τ_g, and δ_g the degree of energy barrier asymmetry (between 0 and 1).

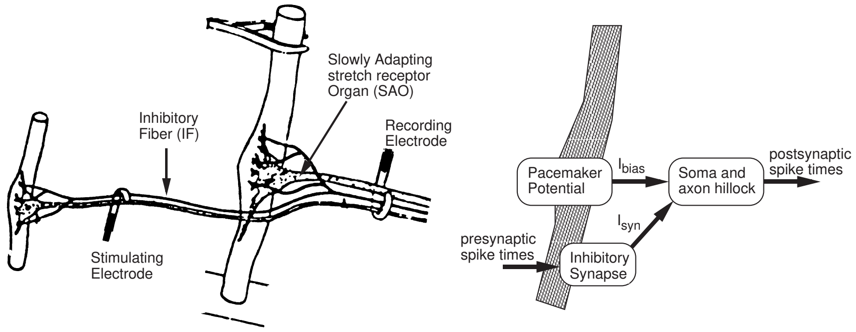

Fig. 1. The crayfish stretch receptor experimental setup (left) and the modified permeability model (right).

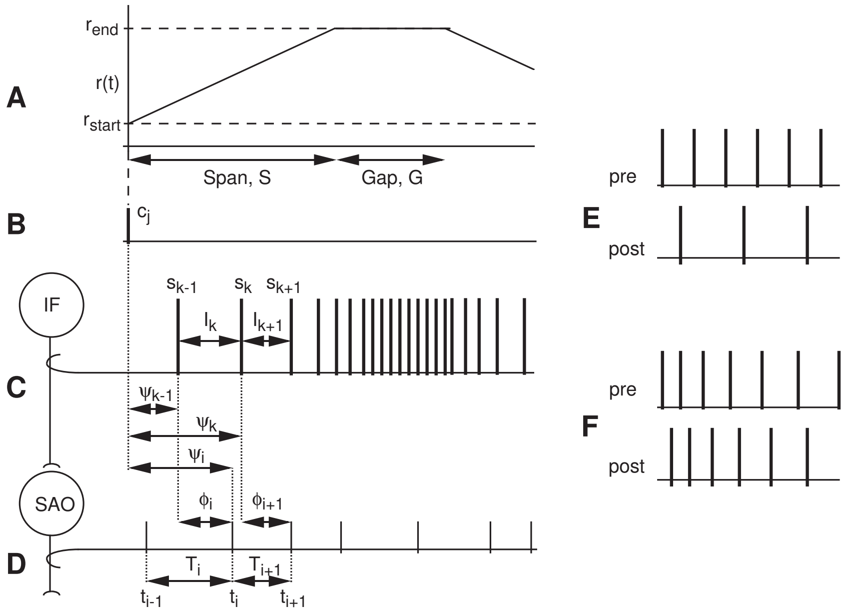

Fig. 2. Transient generation and definition of terms.

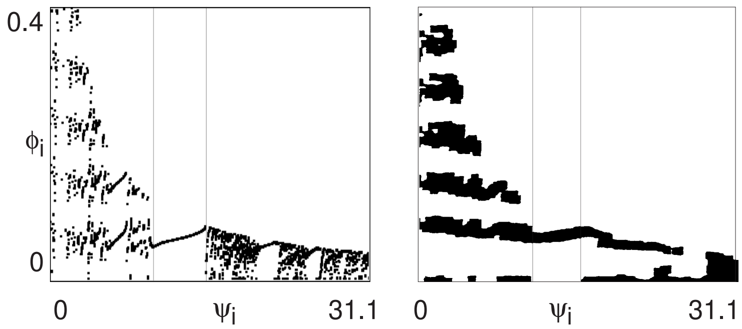

Fig. 3. Phase pooled graphs showing transient responses of SAO (right) and simulation (left). Transient was accelerating ramp, 39ms $\leq I_k \leq$ 1.667s, $S = 31.1$s. Natural firing interval $N = 84$ms.

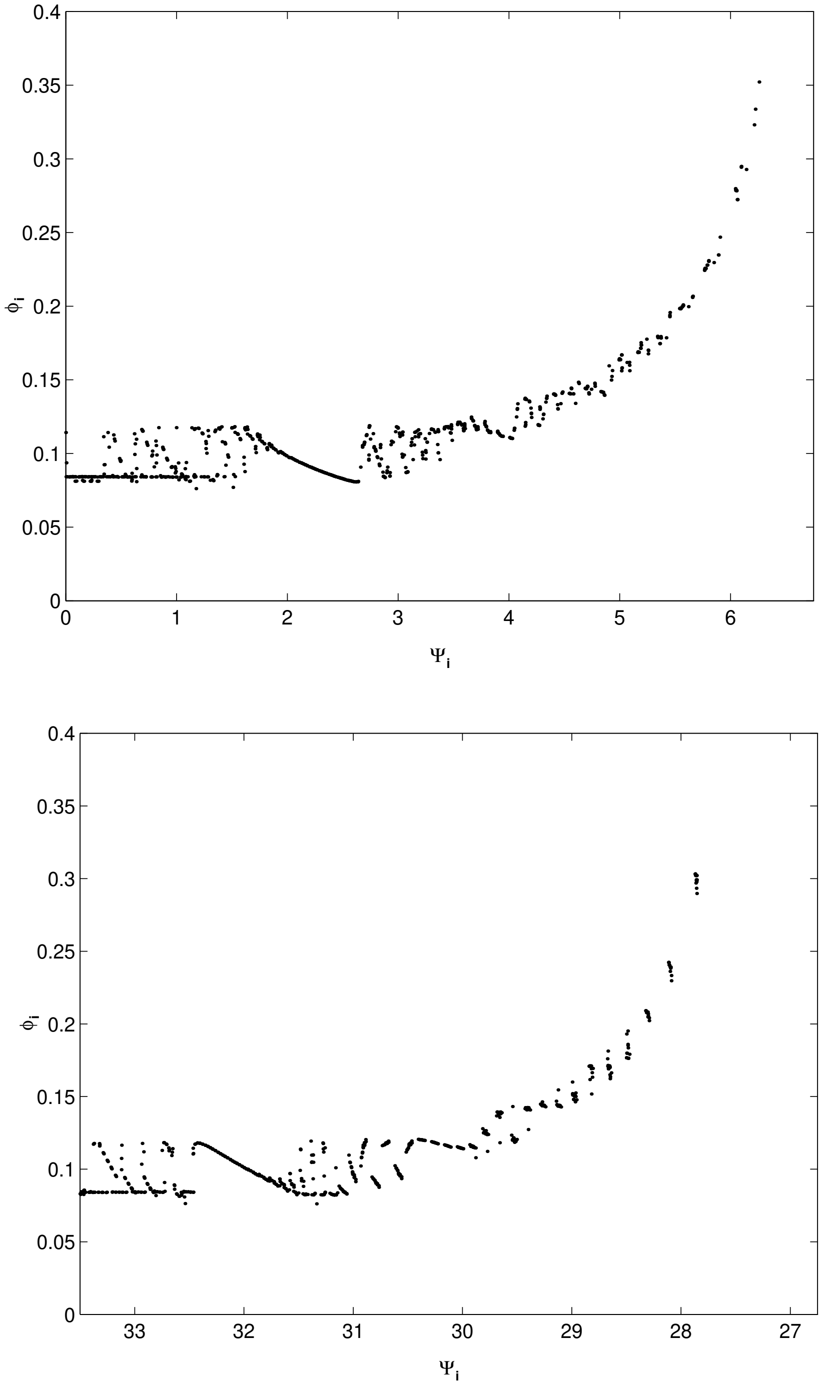

Fig. 4. Phase pooled graphs showing accelerating (top) and decelerating (bottom) transient responses of simulation. Transient parameters: $33.3\text{ms} \leq I_k \leq 333\text{ms}$, $S = 6.75\text{s}$, $G = 20\text{s}$. Natural firing interval $N = 84\text{ms}$.

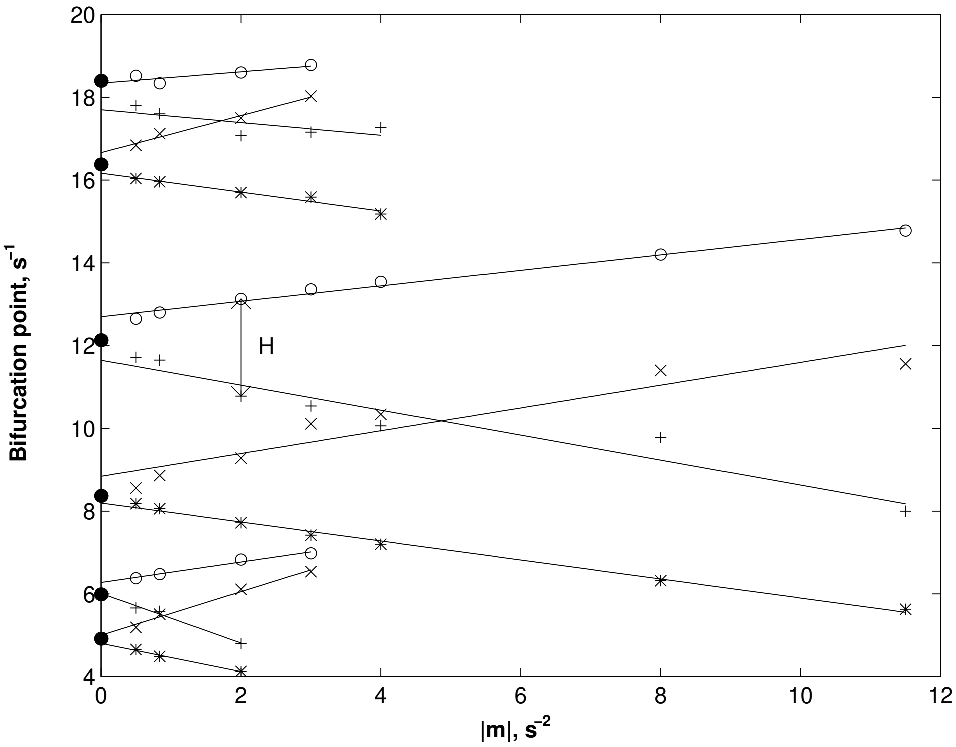

Fig. 5. Bifurcation points bounding 1:2, 1:1, and 2:1 alternations for accelerating ($\circ$, $\times$) and decelerating ($+$, $*$) transients as a function of transient slope. Boundaries of 1:2 and 2:1 only plotted for values of $|m|$ for which the behaviors could be positively identified. Hysteresis (H) caused by non-coincident bifurcations.

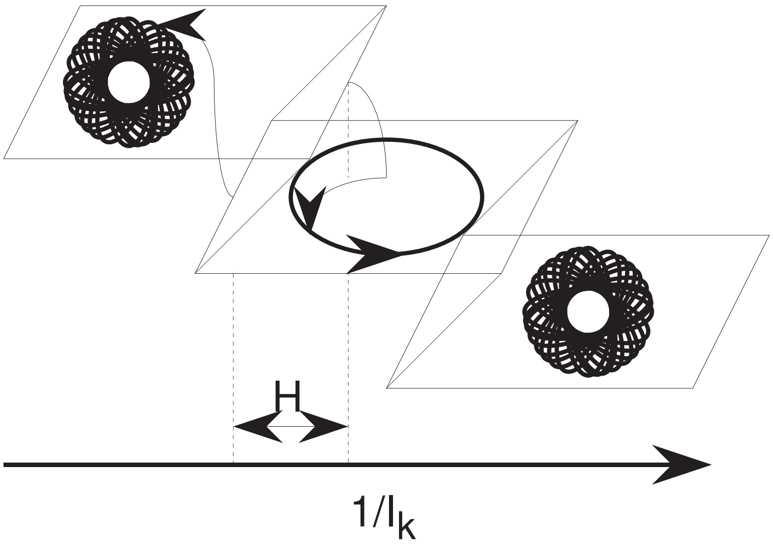

Fig. 6. Hysteresis (H) and bifurcation staircase curve for one value of $|m| > 0$, showing 1:1 alternation and neighboring behaviors.

TABLE I

Delays computed from the slopes of the lines in Fig. 5. Also y-intercepts of lines, actual bifurcation points for pacemaker $(m = 0)$ driving, and correlation coefficients.

Alt	Symbol	δ (ms)	y-int	r_θ	r
1:2	$\circ$	246	6.28	5.99	0.9889
	$+$	599	6.01		0.9911
	$\times$	526	5.00	4.92	0.9932
	$*$	342	4.81		0.9948
1:1	$\circ$	187	12.7	12.13	0.9928
	$+$	302	11.6		0.9633
	$\times$	275	8.84	8.37	0.9441
	$*$	230	8.20		0.9968
2:1	$\circ$	137	18.3	18.4	0.8563
	$+$	155	17.7		0.7329
	$\times$	448	16.7	16.38	0.9920
	$*$	229	16.2		0.9809